Reliability Assessment Of AlGaN/GaN HEMTs on the SiC Substrate Under the RF Stress

Niemat Moultif, Olivier Latry, Eric Joubert, Mohamed Ndiaye, Christian Moreau, Jean-François Goupy, and Patrick Carton

***Abstract*—This article reports a reliability study on AlGaN/GaN high-electron-mobility transistors under the RF stress. It shows a stabilization of the gate contact after the aging test. However, the degradation of RF performances and dc parameters is noticed. The degradations are mainly due to bulk traps located between gate–source or gate–drain and caused by hot-electron effects. The trap-related phenomena results in a reduction of the drain current and RF output power accompanied with transconductance degradation and pinch-off shift. These traps are characterized by gate-lag and drain-lag measurements and spectral photon emission microscopy. Photo emission measurements reveal an inhomogeneous distribution of light and the presence of native traps that could be related to crystallographic defects such as dislocations or impurities.**

***Index Terms*—Gallium Nitride (GaN), high-electron-mobility transistors (HEMTs), photon emission microscopy (PEM), RF stress, reliability.**

I. Introduction

THE physical properties of gallium nitride, i.e., wide bandgap, high saturation electron velocity, and high mobility [1], make the AlGaN/GaN devices interesting candidates for the next generation of power electronics, in particular, for high-frequency and high-power applications [2]. However, this young technology still suffers from reliability issues. Many failure mechanisms have been reported in the literature such as inverse piezoelectric effects, hot-electron effects, and thermally activated mechanisms like ohmic contact degradation or the delamination of passivation [3]–[6]. One of the most dangerous failure mechanisms that continue to limit the performance and reliability of these GaN-based high-electron-mobility transistors (HEMTs) is the prominent trapping phenomena. In the last decades, many studies have been dedicated to investigating the trapping effects of this technology [7]–[9]. The presence of traps in various locations such as surface or barrier or buffer layer of the device degrades the dynamic and the static performance [10], [11]. They could cause microwave output power drop, current collapse, transconductance-frequency dispersion, gate lag (GL), and drain lag (DL) [12]–[14]. An efficient way to evaluate the GaN HEMT reliability is using reliability tests, which include storage tests and short-term and long-term reliability tests, on both dc and RF conditions. These tests aim to better understand the degradation mechanisms and the failure mechanisms that are mainly affecting the device performances, which will contribute to improving the maturity of the technology.

In this article, the RF-stress examination is performed on AlGaN/GaN HEMTs to investigate their stability and their performance under a continuous power operation. The main results of an aging campaign on AlGaN/GaN HEMT devices are reported. Photon emission microscopy (PEM) analysis is presented to understand the failure mechanisms and to provide a feedback on the development and the processing quality of these transistors. This article first presents the experimental setup of the continuous wave (CW) at a 3-GHz aging bench. Then, the characterization results with PEM are presented and discussed. Finally, the conclusion summarizes impacts of the CW-RF stress on the reliability of the aged AlGaN/GaN components.

Manuscript received July 6, 2020; revised October 20, 2020; accepted November 27, 2020. Date of publication December 2, 2020; date of current version March 5, 2021. This work was supported by the French Defence Procurement Agency (DGA) under Contract 2015 91 0907. Recommended for publication by Associate Editor A. Lindemann. *(Corresponding author: Niemat Moultif.)*

Niemat Moultif, Olivier Latry, and Eric Joubert are with the Materials Physics Group Laboratory, UMR CNRS 6634, University of Rouen Normandy, 76801 St Etienne de Rouvray, France (e-mail: niemat.moultif@gmail.com; olivier.latry@univ-rouen.fr; eric.joubert@univ-rouen.fr).

Mohamed Ndiaye is with CEVAA, Technopole du Madrillet, 76800 Saint Ètienne de Rouvray, France (e-mail: m.ndiaye@cevaa.com).

Christian Moreau is with DGA-MI, 35998 Rennes, France (e-mail: christian.moreau@intradef.gouv.fr).

Jean-François Goupy is with Thales LAS France, 76520 Ymare, France (e-mail: jean-francois.goupy@thalesgroup.com).

Patrick Carton is with Thales Global Services, 78140 Velizy Villacoublay, France (e-mail: patrick.carton@thalesgroup.com).

Color versions of one or more figures in this article are available at https://doi.org/10.1109/TPEL.2020.3042133.

Digital Object Identifier 10.1109/TPEL.2020.3042133

II. Experimental Setup

A. Device Under Test (DUT)

The devices studied in this work are commercial AlGaN/GaN HEMT power bars on the SiC substrate with voltage and current rating of 30 V and 5 A, respectively. The device is in a ceramic package and designed for the S-Band. The transistor consists of 20-gate fingers with a total gate development of 5.5 mm. The transistor gate has a T shape and a length of 0.25 μm. A field plate with a source termination is used in this transistor. In order to examine this device, a power amplifier has been designed in the AB class [15]. The design of the amplifiers allows *in situ* measurements to enable measurements (*I–V* pulsed characterizations and diode measurements) without unplugging the amplifiers and losing the RF calibration of the bench (see Fig. 1).

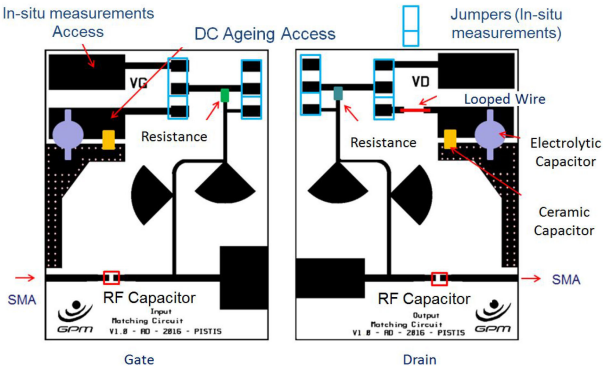

Fig. 1. Circuit diagram for the designed RF amplifier.

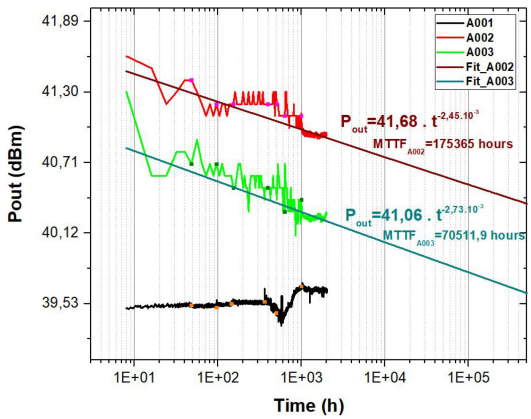

Fig. 2. Evolution of the RF output power.

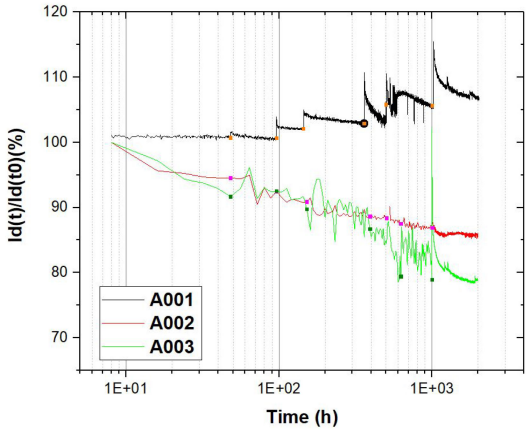

Fig. 3. Relative average drain current evolution during stress tests in percentage.

B. Test Description

The test bench used in this work can address aging both in L-Band ([1; 2] GHz) [16] and S-Band ([2; 4] GHz) [17]. The RF test conducted on this study is in the CW mode at a 3-GHz operating frequency. The input power is adjusted to have a compression around 3 dB for the device A001 and 6 dB for the devices A002 and A003. The DUTs have been run at a quiescent current (I_{dq}) corresponding to a deep class-AB amplification close to $V_{\mathrm{ds(max)}}$ ($V_{\mathrm{DS0}} = 30$ V and $I_{dq} = 1.09$ mA/mm). The amplifiers operate in the saturation region to ensure the stability of the RF output power. All devices were subject to a burn-in before the aging in order to stabilize their dc and RF parameters.

The base plate temperature is adjusted at 120 °C, which according to our estimations corresponds to a junction temperature of 208 °C. The mean junction temperature is estimated using pulsed *I–V* measurements at different temperatures and dissipated powers [18] and checked with IR thermography. For this test, one of the devices underwent only a temperature storage test on the bench without any dc or RF signal during the entire test "A004_Storage."

Several parameters are monitored and analyzed during the aging test in order to evaluate the reliability of the DUTs, including the input, output, and reflected power, the case temperature, in addition to the average voltages and currents on the drain and on the gate. The aging is stopped at logarithmic intervals for interim measurements, and the curves are corrected at each stop to remedy the relaxation problem. The interim measurements include the following.

1) DC characterization: Pulsed $I_{\mathrm{DS}} = f(V_{\mathrm{DS}}, V_{\mathrm{GS}})$, Schottky characterization, transconductance (G_m), and threshold voltage (V_{th}).
2) RF characterization: $P_{\mathrm{OUT}} = f(P_{\mathrm{IN}})$, $\mathrm{PAE} = f(P_{\mathrm{IN}})$, $\mathrm{Gain} = f(P_{\mathrm{IN}})$, and $I_G = f(P_{\mathrm{IN}})$.

These measurements have been carried out at t0, t0+Burn-in, 48, 96, 144, 500, 1000, and 2000 h. The test is planned for a total duration of 2000 h unless a failure occurs for all the DUTs. In this case, a device is considered in failure if a drop of 1 dB is noticed at the output power.

III. Aging Test Results

A. Electrical Characterizations

The first noticeable element from the monitoring of the electrical parameters during the aging is the correlation between the output power (P_{out}) and the drain current (I_{ds}) variations (see Figs. 2 and 3). It can be noticed from Fig. 2 that a stronger decrease of the output power affects the amplifiers operating with a higher gain compression (A002 and A003). The drop in P_{out} is close to 0.5 dB for these amplifiers. The amplifiers A002 and A003 also show a significant decrease in the drain current (see Fig. 3) especially the device "A003" that seems to be the most impacted by the stress (drop of 22%). However, the amplifier that underwent the lower gain compression (3 dB) (device "A001") shows a slight increase of P_{out} and I_{ds}.

For A002 and A003, the law of P_{out} diminution is of the form $P_{\mathrm{out}} = at^b$ with $a = P_{\mathrm{out}}(t = t_0)$ and b equal to -0.00245 and -0.00273 for A002 and A003, respectively. According to this law, the predicted mean time to failure (MTTF), using $\Delta P_{\mathrm{out}} = -1$ dB as the failure criterion, is equal to 175 365 h and 70511.9 h for A002 and A003, respectively. We see that the MTTF of A002 is longer by a factor of 2.5, which appears consistent with the drain current variations of the two devices.

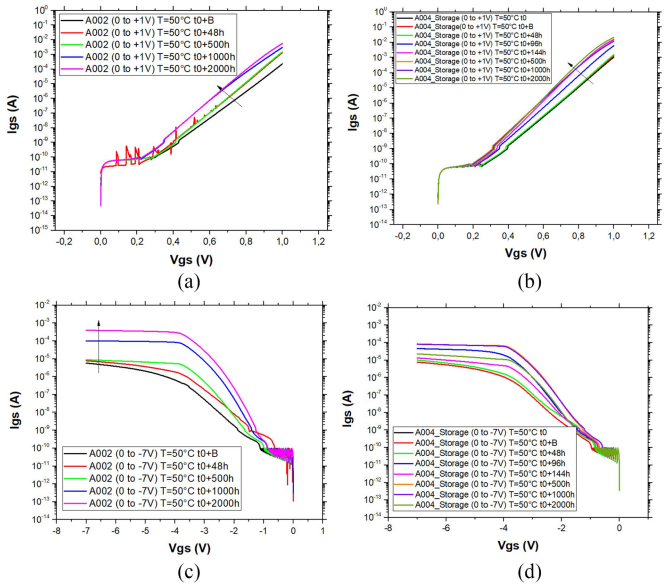

Fig. 4. Schottky characteristics of DUT "A002" and "A004_Storage." (a) and (b) Forward characteristic. (c) and (d) Reverse characteristic.

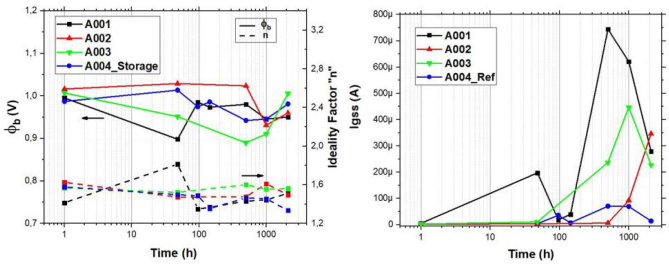

Fig. 5. Evolution of the Schottky barrier height and the ideality factor during the aging test.

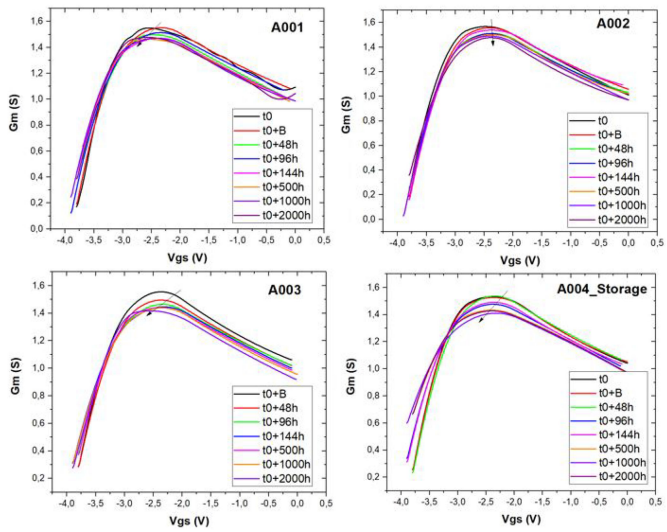

Fig. 6. Evolution of the transconductance during the stress.

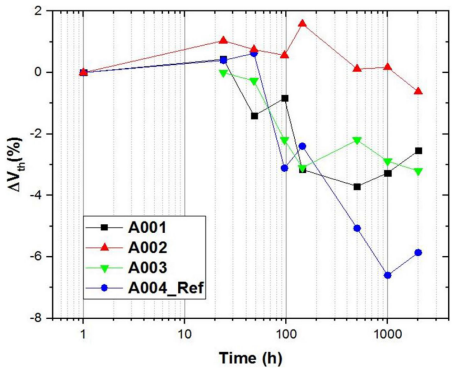

Fig. 7. Evolution of the relative threshold voltage variation during the stress.

The output power and drain current variations may be a consequence of an evolution of the GaN structure; however, in order to give a more accurate conclusion and to gain more information, complementary measurements ("interim measurements") during the ageing test are mandatory.

The gate design and process is a major reliability issue in AlGaN/GaN HEMTs [19]. The Schottky junction is considered among the most sensitive part on HEMT devices, which makes the follow-up of its characteristic fundamental during an aging test. This contact is precisely characterized in forward and reverse diode during interim measurements (see Fig. 4). The Schottky parameters [Schottky barrier (Φ_b), ideality factor (n), and the reverse gate leakage current ($I_{\rm gss}$)] are extracted (see Fig. 5) from the forward and reverse Schottky characteristics. It can be noticed from Schottky characterizations that the ideality factor fluctuates over time, whereas the Schottky barrier shows a decrease at the early hours of the stress and then increases. Unlike Φ_b, the leakage current increases at first and then decreases. The variation of these parameters shows a stabilization of the Schottky contact, which takes place at different times depending on the devices. The stabilization is earlier for the device "A001" and comes later for the amplifiers "A002," "A003," and "A004_Storage."

Next, the transconductance characteristics ($G_m - V_{\rm gs}$) are studied in detail for each device (see Fig. 6). Fig. 6 shows that the maximum of G_m ($G_{m(\max)}$) decreases during the aging for all the devices. In addition to a decrease of $G_{m(\max)}$, the transconductance curves of devices "A001," "A003," and "A004_Storage" present a negative shift. The decrease of $G_{m(\max)}$ is attributed to traps located between gate and source (G–S) or gate and drain (G–D) at the AlGaN/GaN interface [12], [20], [21]. However, the lateral translation of the transconductance curve is related to the threshold voltage $V_{\rm th}$ shifts caused by traps located under the gate fingers [12], [20], [21]. Fig. 7 shows the evolution of the relative threshold voltage variation during the stress. It seems that the threshold voltage of the devices "A001," "A003," and "A004_Storage" shows a drift toward more negative values during the stress. However, the threshold voltage of the device "A002" is relatively stable. These results are in a good correlation with G_m variations. The positive and negative pinch-off voltage shifts are common degradation of GaN HEMT devices and have been noticed during the dc stress [22] and RF stress [23]. The $V_{\rm th}$

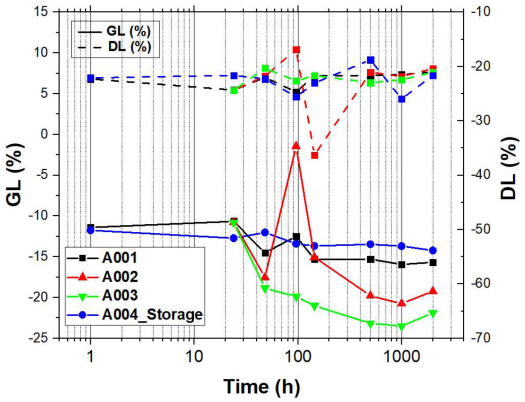

Fig. 8. GL and DL evolution during the stress.

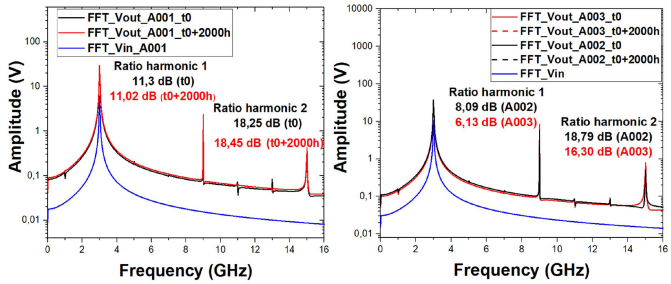

Fig. 9. Input and output spectrum of "A001," "A002," and "A003" amplifiers before and after the aging.

shift could be caused by the charging of traps or by the generation of charged traps below the gate contact. For the first mechanism, the degradation can be fully recovered by UV light illumination or temperature storage, while for the second mechanism, degradation can be, sometimes, partly recovered by temperature storage [24]. In our case, the degradation for devices that underwent the RF stress was irreversible. Therefore, the drain current degradation is probably caused by emission/capture of electrons from slow traps or/and by hot-electron-induced slow trap generation at the AlGaN/GaN interface or at the SiN/GaN cap interface [24], [25].

The first conclusion that could be drawn is that the stress seems to be causing a variation in the quantity of traps at different locations.

1) For the devices "A001," "A003," and "A004_Storage": The traps are located under the gate and between G–S or D–S at the AlGaN/GaN interface (shift of V_{th} and drop of $G_{m(\max)}$).
2) For the device "A002": The traps are only located between G–S or D–S at the AlGaN/GaN interface (drop of $G_{m(\max)}$).

The evaluation of the trapping state is then essential for a better interpretation of the results. In order to better investigate the trapping phenomena in GaN HEMTs, "GL" and "DL" measurements are conducted. Pulsed *I–V* measurements were performed at three different quiescent points ($V_{\text{GS}q}/V_{\text{DS}q}$: 0 V/0 V; −7 V/0 V; and −7 V/30 V), then GL and DL ratios are extracted according to the method explained in [26]. Fig. 8 shows the evolution of GL and DL during the aging test. It can be noticed that the DL fluctuates over time, whereas the GL increases after the aging test. The increase of GL is more important for the devices that underwent higher compression ($\sim$ 10% for "A002" and "A003" versus 4% for "A001"). The GL is principally due to two mechanisms [12], [27]. The first one is the virtual gate mechanism, which is associated with the increase of ionized donor states located on the surface between the gate and the drain electrodes [28]. The second mechanism is related to the positive shift of the pinch-off voltage for negative gate bias, which is due to charge trapping under the gate [12]. This states that the origin of the GL variation of devices "A001" and "A003" could be the virtual gate mechanism or/and the positive shift of V_{th}. Since the V_{th} of the amplifier "A002" is stable, the GL variation of this device could only be attributed to the virtual gate mechanism. However, the GL variation of the amplifier "A004_Storage" could only be related to the positive shift of V_{th} because the device was stored under 120C without dc and RF bias. In the literature, traps that influence the DL transient response of GaN-based HEMTs are presumed to be located in the buffer [14], while traps responsible for the GL could be located at the surface [12], [29] or in the bulk (AlGaN barrier or GaN buffer) [13], [30], [31]. This suggests that the stress caused an evolution of the quantity of traps in the buffer at the gate edges or/and under the gate.

B. Interpretation

It is obvious that the change in RF and dc indicators are more pronounced at elevated compression levels certainly due to higher nonlinear effects. Indeed, we studied the linearity of the amplifiers by analyzing the response (V_{out}) to a single input signal (V_{in}) at the fundamental frequency (3 GHz) (see Fig. 9). The amplifiers are set to saturation that justify their nonlinearity and the presence of the spectral harmonics. Therefore, it can be seen from Fig. 9 that the ratio between the levels of the fundamental component and the first (or the second) harmonics suggest that nonlinearity effects are less pronounced at lowered compression levels (8,09 dB for A002 and 6,13 dB for A003 versus 11,3 dB for A001). Moreover, it can be concluded from Fig. 9 that the aging test does not have any impact on the linearity of the amplifiers "A002" and "A003" because the spectrums before and after the stress coincide perfectly. For the "A001" amplifier, a very slight increase of the level of the V_{out} spectrum is observed after the stress.

The correlation between the drain current and RF power variations is a well-known signature of GaN technologies [23]; this suggests that the RF variation at the output of the devices is not related to a degradation of the two-dimensional electron gas (2DEG) channel, but more likely to a change of the gated zone (under or below the 2DEG) [32].

During the RF stress at low compression (3 dB), the device "A001" shows a slight increase of the GL (4%) and V_{th} (4%), accompanied with a decrease of $G_{m(\max)}$. This reflects a slight evolution of traps located under the gate and between G–S or G–D at the AlGaN/GaN interface. The effect of these traps

seems to be compensated by an early stabilization of the gate contact that helps improving the RF performance of the device and increase slightly the output power and the drain current. For the device "A002" operating at a high compression (6 dB), V_{th} is stable, while $G_{m(\max)}$ decreases and GL increases (8.5%) with the stress. This states that the stress causes an evolution of the traps distributed between G–S or G–D at the AlGaN/GaN interface. The reduction of the output power and drain current seems to be due to GL effects that becomes more important after the stress [33], [34]. According to Paine[5], [6], the change of peak transconductance is caused by hot-electron effects. When the device is driven in ON-state at high V_{DS}, the 2DEG channel of electrons is accelerated by a high electric field and reaches a high energy, which make the electron "hot." For the device "A003" operating at a high compression (6 dB), $G_{m(\max)}$ decreases, while V_{th} and the GL increases (4% and 10%, respectively) with the stress. The change of V_{th} is attributed to electron trapping phenomena near the gate [5], [35]. This means that bulk traps located under the gate and at the G–S or G–D are the cause of the RF output power and drain current degradations. These traps are induced by hot-electron effects. Indeed, the hot electrons can overcome energy barriers and dissipate their extra energy in collision with the crystal. Thus, they can create defects or dangling bonds that may act as deep levels or traps [20]. For these reasons, hot electron can be the origin of the observed degradations and trapping phenomena within the passivation or GaN layers. Both devices "A002" and "A003" have shown a stabilization of the gate contact (the "A003" was earlier than the "A002"), but its effect cannot be noticed on the device performance because the impact of hot electrons is more predominant.

However, the degradation mechanism cannot be associated only to high electric field conditions, because some degradations have also been found on the device stored under 120 °C (no dc and RF bias). This means that there is a strong contribution of high electric field conditions and high temperatures. Consequently, degradation can be electrically (energy levels) and thermally activated.

Indeed, the thermal storage stress at 120 °C of the device A004_Storage results in an increase of V_{th} (7%), which correlates with a negative shift of the G_m curve. A degradation of the transconductance peak can be seen, while the GL slightly increases by 2.5%. This states that the thermal storage causes trapping effects that took place on the device surface both under the gate and in the access regions [32], [36]. These effects are not permanent and can be recovered after a time of inactivity. However, traps phenomena could explain the general evolution of the electrical parameters but it does not explain why the device "A004_Storage" shows the largest threshold voltage shifts [an increase of *V*th (7%)], while the GL increases only by 2.5%. Thermal storage must have caused another mechanism that compensates the GL increase. What might cause the degradation here is still not clear. Some research groups [37]–[39] speculate that the dc and RF degradations at a high temperature storage (> 300 °C) might be induced by the change of surface charge distribution between the nitride passivation and the AlGaN barrier layer, metal contact degradation, isolation, or imperfect material quality on AlGaN/GaN HEMTs subjected to a thermal stress.

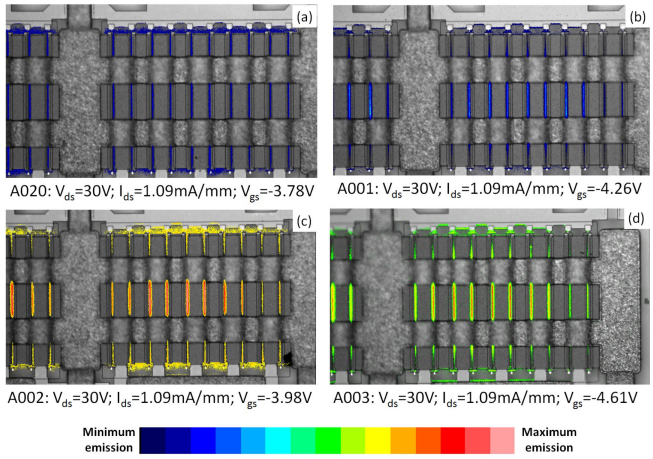

Fig. 10. Comparison of PE images in the ON-state mode ($I_{\text{ds}} = 1.09$ mA/mm). (a) A020 reference device. (b) A001 aged. (c) A002 aged. (d) A003 aged.

The Schottky characterizations of the A004_Storage device suggest that the thermal storage causes a stabilization of the gate contact. Zhao *et al.* [40] report that the temperature plays a significant role in the cleaning of gate contacts, which may lead to a reduction of the leakage current.

For hot-electron evaluation and in order to investigate possible physical degradations, PEM measurements are conducted. The ceramic cap of the transistor frame has been removed to allow die inspection with PEM.

C. PEM Characterizations

PEM is a powerful failure analysis tool that has proven its efficiency in many reliability studies of AlGaN/GaN HEMTs. In the ON-state operating mode, PEM was used to reveal the presence of impact ionization in AlGaN/GaN HEMTs [41] and to localize electronic traps produced in the devices during the stress [42]. In the OFF-state, PEM was used to monitor the degradation of AlGaN/GaN HEMT devices [43] and to analyze the stress-induced percolation path [44]. This technique was also used to evaluate the impact of the surface oxidation [45]. In this article, PEM analysis on new and stressed AlGaN/GaN HEMTs is presented in the ON-state and the OFF-state operation modes.

PEM observations have been performed using the HAMAMATSU microscope PHEMOS 1000. Images are acquired under the same dc bias conditions with the same exposition time (10 s), detector sensitivity, and color scale. In the ON-state operation mode ($V_{\text{ds}} = 30$ V and $I_{\text{ds}} = 1.09$ mA/mm), the photoemission (PE) signature of the new reference device "A020" appears quite uniform over the entire structure with a localization of the emission along the 20 gate fingers as shown on Fig. 10. Compared to the reference device, the aged devices reveal a different light distribution. An inhomogeneous light emission is observed along each gate finger with a stronger intensity at the center of fingers. This is due to the nonuniformity of the temperature distribution, which is higher in the center of the fingers as it has been observed from infrared microscopy measurements. In addition, the electroluminescence produced

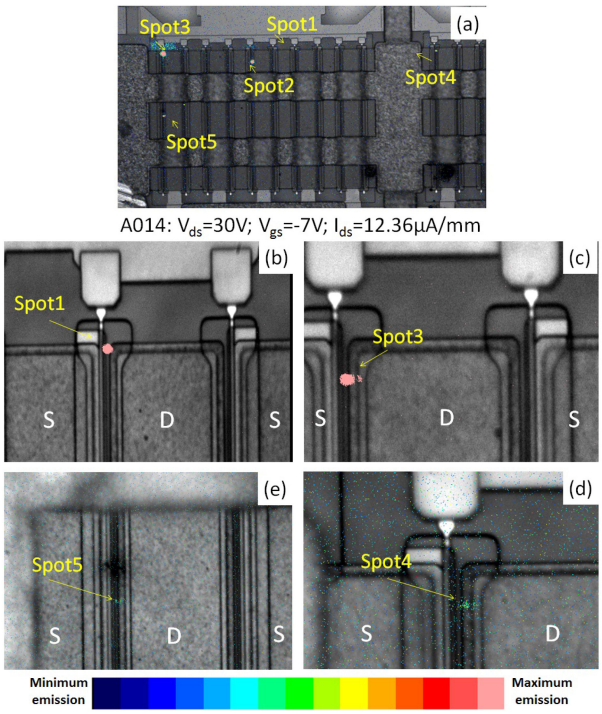

Fig. 11. Spots localization of a new device "A014" operating in the OFF-state mode.

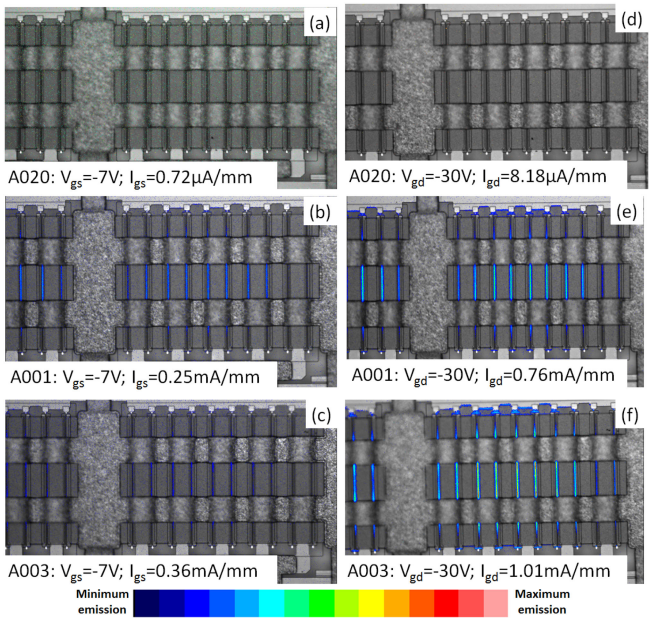

Fig. 12. Comparison of PE images in the diode mode. (a)–(c) G–S diode: $V_{gs} = -7$ V. (d)–(f) G–D diode mode at $V_{gd} = -30$ V.

is not uniform on the surface of the device, and the central fingers are brighter than the peripheral fingers. This suggests that the degradation is not uniform on the device and that the pinch-off voltage of the central fingers has increased. Indeed, the light intensity is related both to electric field and current flow, which means that the drain current distribution among fingers is probably also irregular. As the gate voltage V_{gs} is uniformly distributed, the pinch-off voltage may have shifted more negatively at the center of the die rather than at the edge.

In the OFF-state operating mode ($V_{ds} = 30$ V and $V_{gs} = -7$ V), the reference device ("A014") presents a low leakage current (12.36 μA/mm), and the PEM measurements reveal the presence of many "hot spots" (see Fig. 11). These hot spots may be due to the presence of native intrinsic crystal defects, with local change in the electric field [46] or a current leakage path. PEM measurements are realized with a higher magnification (X100) in order to localize more precisely the position of these hot spots. The PE image in Fig. 11 shows that the PE spots are located at the edge of the gate on the drain side. These spots will be analyzed by the spectral PEM (SPEM) technique to determine their origin.

Compared to the new device, the aged amplifiers present a different behavior in the OFF-state operating mode. Indeed, in this mode, they produce a luminescence along the gate fingers similar to the one produced in the ON-state operating mode. The luminescence is nonuniform and some discrete and very localized hot spots can be noticed. The variation in the PE response after aging is probably related to the increase in the reverse gate leakage current and to hot-electron effects. Indeed, the reverse gate leakage current being higher on the aged devices (few milliamperes) for the same dc bias (−7 V, 30 V), the PE signature is, therefore, localized along the fingers because of the current flow. The illumination is higher in the center of the devices because the temperature and the energy of the electrons are greater in the central areas. The PE distribution reveals, here, the leakage pathways resulting from a gate leakage current assisted by traps.

The PE characterizations were performed also in a diode mode: G–S diode mode [$V_{gs} = -7$ V; see Fig. 12 (a)–(c)] and G–D diode mode [$V_{gd} = -30$ V; see Fig. 12 (d)–(f)]. From Fig. 12, we notice great similarities on all aged devices. In the G–S diode mode, no particular signature was observed on the new device due to the low leakage current ($I_{gs} = 4\ \mu$A). However, the aged devices that present a higher leakage current (few milliamperes) show an emission on the central fingers of the die, located on the central part of the fingers. The aged devices in the reverse-biased G–D diode mode present a light emission response almost identical to the one obtained in the OFF-state operating mode. The only difference lies in with the intensity of the light emitted signal, which is stronger in the OFF-state mode.

1) SPEM Analysis: SPEM is used to extract the fingerprint of the defect emissions of our DUT. A diffraction grating was used as a spectrometer and placed in the optical path of the PE microscope, between the objective lenses and the charge-coupled device (CCD) detector [26]. The reference device spots have been analyzed with the SPEM technique and compared to the stressed device spots (see Fig. 13). The PE spectrum is extracted from the diffraction line connecting the orders "0" and "1" of the diffraction pattern. Fig. 14 presents the PE spectrum of the new device spots and the stressed devices spots obtained in the OFF-state mode.

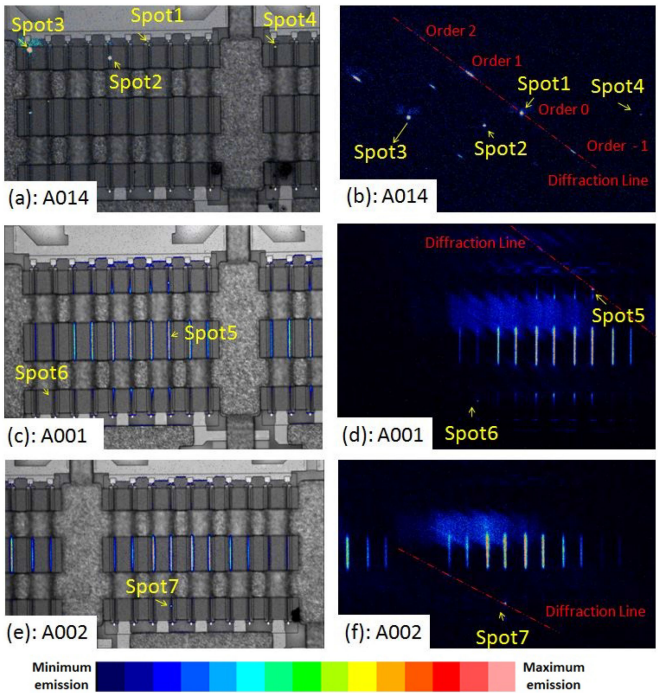

Fig. 13. Spot localization of: (a) A014; (b) A001; and (c) A002. Spots diffraction of: (d) A014; (e) A001; and (f) A002.

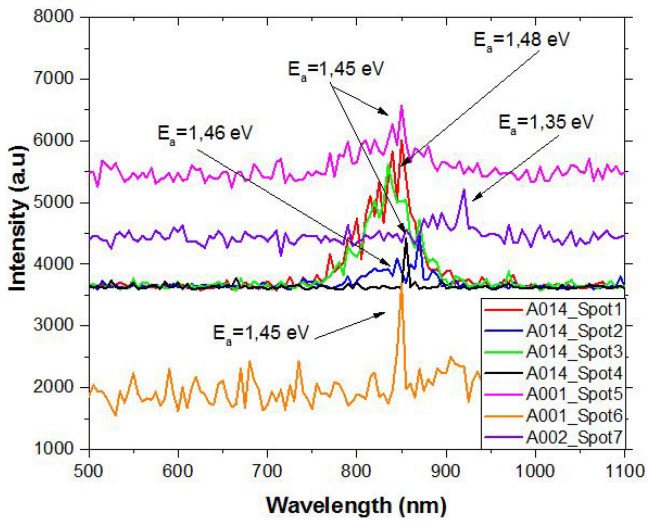

Fig. 14. PE spectrum.

We note great similarity between the spectral distributions of spots "1" and "3" of the new device, which range between 770 and 890 nm. These distributions are centered on 835 nm, which corresponds to an energy level of 1.48 eV. The spectrum of the spot "4" of the new device indicates an almost monochromatic emission centered on 855 nm, which corresponds to an energy level of 1.45 eV. The spectrum of the spot "2" of the new device is narrower than the spectrum of spots "1" and "3." It ranges between 790 and 885 nm and its central component is located at 848 nm corresponding to 1.46 eV. For spots "1," "2," and "3," other peaks are observed at different wavelengths.

TABLE I
POSITIONS OF THE PEAKS OBSERVED ON THE SPECTRA OF THE SPOTS OF THE DEVICES "A014," "A001," AND "A002"

Peaks	1	2	3	4	5	6	7	8	9	10	11	12	13	14	15	16	17
Spot 1	770nm 1.61eV			800nm 1.55eV		815nm 1.52eV		825nm 1.5eV	840nm 1.48eV		850nm 1.45eV						
Spot 2					805nm 1.54eV		820nm 1.51eV		835nm 1.48eV	845nm 1.46eV		860nm 1.44eV	870nm 1.42eV	885nm 1.4eV			
Spot 3		778nm 1.59eV	790nm 1.57eV				820nm 1.51eV		835nm 1.48eV		855nm 1.45eV		870nm 1.42eV	885nm 1.4eV			
Spot 4											855nm 1.45eV						
Spot 5											850nm 1.45eV						
Spot 6											850nm 1.45eV						
Spot 7													875nm 1.42eV	885nm 1.4eV	895nm 1.38eV	920nm 1.35eV	915nm 1.35eV

Table I summarizes the positions of the peaks of each spot. Peaks at 1.4, 1.42, 1.48, and 1.51 eV can be noticed to occur both on the spectrum of spots "2" and "3." This means that the two spots have components of the same physical origin. We also note that the peak at 1.45 eV is present for the spots "3" and "4." The peak at 1.46 eV has been observed by SPEM by Glowacki *et al.* [47] on new AlGaN/GaN HEMTs. The authors [47] also observed that the same peak and another peak at 1.59 eV on AlGaN/GaN HEMTs degraded following the dc stress. They claim that the origin of these traps may be attributed to the following:

1) intraband transitions of highly energetic electrons due to diffusion by charged centers;
2) intraband transitions of electrons assisted by phonon;
3) direct transitions of electrons between bands;
4) recombination via deep levels.

In [48], the authors found with deep-level transient spectroscopy (DLTS) a peak at 1.48 eV on Schottky InAlN/GaN. Sun *et al.* [11] observed with DLTS and DLOS a 1.5-eV trap on AlGaN/GaN HEMTs stressed by a dc test. The authors[11] suspect that this trap is the cause of the ON-state resistance R_{ON} variation following the stress. Arehart *et al.* [49] found the same trap by DLOS on Schottky AlGaN, but the origin of this trap is still unknown. In [50], the authors found a trap at 1.55 eV by DLOS on AlGaN/GaN HEMTs but they could not identify its origin. The shape of the spectrum of spots "1," "2," and "3" is similar to the one obtained by Shigekawa *et al.* [51] on AlGaN/GaN HEMTs but the dynamics of the spectrum is different. The spectrum found in [51] extends between 500 and 800 nm with a peak at 670 nm (1.85 eV) or 690 nm (1.8 eV) depending on the value of V_{gs} ($V_{gs} = -4$ V and $V_{gs} = 0$ V, respectively). The emission is attributed to the intraband transition of the channel electrons located at the edge of the drain where the field is high. Zanoni *et al.* [3] report a PE spectrum of an AlGaN/GaN HEMT that ranges between 1.2 and 2.4 eV. The authors claim that the light emission is caused by intraband transitions of highly energetic electrons.

For the aged amplifier "A001," two spots were observed in the OFF-state mode [see Fig. 13(c)]. The two spots were analyzed in SPEM in order to identify their nature [see Fig. 13(d)]. Even if the spot "5" has a wider spectrum than the spectrum of the spot "6," we note that the two spectra are centered on the same wavelength of 850 nm corresponding to 1.45 eV. This trap was also obtained on the reference device, which means that it is probably a native defect.

On the aged amplifier "A002," a spot was observed in the OFF-state mode [see Fig. 13(e)]. The spectral PE analysis of this spot shows an extended spectrum between 870 and 935 nm, centered on 915 nm (1.35eV) with peaks at 875 nm (1.42 eV), 885 nm (1.4 eV), 895 nm (1.38 eV), and 920 nm (1.35 eV). Defects at 1.4 and 1.42 eV have already been observed on the reference device, which means that they are probably native defects. The peak at 1.35 eV has already been observed by Moultif *et al.*[26] on new and aged AlGaN/GaN HEMTs, and according to the literature, it corresponds to an interstitial carbon defect [10], [52]–[54].

IV. Conclusion

This article presents a reliability study on an AlGaN/GaN HEMT under the RF stress. The RF stress on AlGaN/GaN HEMTs under a continuous power operation induces variations in the dc and RF performances that are most significant for the most compressed devices (drain current and RF output power drop, positive shift of the threshold voltage, decrease of the maximum transconductance peak, and increase of GL). These variations are attributed mainly to hot-electron effects and traps located on the bulk under the gate or between G–S or G–D, which is confirmed by PE. Failure analysis on aged devices shows that PE distribution is strongly inhomogeneous, unlike in the case of reference new devices because the temperature and energy of the electrons are greater in the central areas of the devices. PE spots located at the edge of the gate on the drain side are observed. Spectrally resolved PE measurements from new and aged AlGaN/GaN HEMTs identify 17 wavelengths on this technology of devices. The spectrum of PE from aged devices has additional maxima in the higher wavelength regime. Similar peaks are observed in new samples in the OFF-state operation mode suggesting that the traps are native defects present before and after aging. To provide more information on generated/activated defects and their distribution, A-DCTS measurements would be conducted in the future on other aging campaigns.

Acknowledgment

The authors would like to thank the French Ministry of Defence for the support.

References

[1] M. Meneghini, A. Tajalli, P. Moens, A. Banerjee, E. Zanoni, and G. Meneghesso, "Trapping phenomena and degradation mechanisms in GaN-based power HEMTs," *Mater. Sci. Semicond. Process.*, vol. 78, pp. 118–126, May 2018.

[2] K. J. Chen *et al.*, "GaN-on-Si power technology: Devices and applications," *IEEE Trans. Electron Devices*, vol. 64, no. 3, pp. 779–795, Mar. 2017.

[3] E. Zanoni *et al.*, "A review of failure modes and mechanisms of GaN-based HEMTs," in *Proc. IEEE Int. Electron Devices Meeting*, 2007, pp. 381–384.

[4] G. Meneghesso *et al.*, "Reliability of GaN high-electron-mobility transistors: State of the art and perspectives," *IEEE Trans. Device Mater. Rel.*, vol. 8, no. 2, pp. 332–343, Jun. 2008.

[5] B. M. Paine, "Scaling DC lifetests on GaN HEMT to RF conditions," *Microelectron. Rel.*, vol. 55, no. 12, pp. 2499–2504, 2015.

[6] B. M. Paine, S. R. Polmanter, V. T. Ng, N. T. Kubota, and C. R. Ignacio, "Lifetesting GaN HEMTs with multiple degradation mechanisms," *IEEE Trans. Device Mater. Rel.*, vol. 15, no. 4, pp. 486–494, Dec. 2015.

[7] L. Brunel *et al.*, "Analysis of Schottky gate degradation evolution in AlGaN/GaN HEMTs during HTRB stress," *Microelectron. Rel.*, vol. 53, no. 9, pp. 1450–1455, 2013.

[8] M. Meneghini *et al.*, "Reliability and failure analysis in power GaN-HEMTs: An overview," in *Proc. IEEE Int. Rel. Phys. Symp.*, Apr. 2017, pp. 3B–2.1–3B–2.8.

[9] H. Lakhdhar, "Reliability assessment of GaN HEMTs on Si substrate with ultra-short gate dedicated to power applications at frequency above 40 GHz," Ph.D. dissertation, Université de Bordeaux, Bordeaux, France, Dec. 2017.

[10] A. R. Arehart *et al.*, "Spatially-discriminating trap characterization methods for HEMTs and their application to RF-stressed AlGaN/GaN HEMTs," in *Proc. Int. Electron Devices Meeting*, Dec. 2010, pp. 20.1.1–20.1.4.

[11] W. Sun, C. Lee, P. Saunier, S. A. Ringel, and A. R. Arehart, "Investigation of trapping effects on AlGaN/GaN HEMT under DC accelerated life testing," in *Proc. IEEE Int. Rel. Phys. Symp.*, Apr. 2016, pp. CD–3–1–CD–3–6.

[12] M. Meneghini *et al.*, "Investigation of trapping and hot-electron effects in GaN HEMTs by means of a combined electrooptical method," *IEEE Trans. Electron Devices*, vol. 58, no. 9, pp. 2996–3003, Sep. 2011.

[13] K. De and G. Dutta, "Investigation of trap induced gate lag phenomenon in AlGaN/GaN high electron mobility transistors," in *Proc. 4th IEEE Int. Conf. Emerg. Electron.*, 2018, pp. 1–5.

[14] N. K. Subramani, M. Bouslama, R. Sommet, and J. Nallatamby, "Time domain drain lag measurement and TCAD-based device simulations of AlGaN/GaN HEMT: Investigation of physical mechanism," in *Proc. 14th Eur. Microw. Integr. Circuits Conf.*, 2019, pp. 21–24.

[15] N. Moultif *et al.*, "S-band pulsed-RF operating life test on AlGaN/GaN HEMT devices for radar application," *Microelectron. Rel.*, vol. 100–101, 2019, Art. no. 113434.

[16] O. Latry *et al.*, "A 5000h RF life test on 330 W RF-LDMOS transistors for radars applications," *Microelectron. Rel.*, vol. 50, no. 9, pp. 1574–1576, 2010.

[17] A. Divay, C. Duperrier, F. Temcamani, and O. Latry, "Effects of drain quiescent voltage on the ageing of AlGaN/GaN HEMT devices in pulsed RF mode," *Microelectron. Rel.*, vol. 64, pp. 585–588, 2016.

[18] N. Moultif, A. Echeverri, D. Carisetti, O. Latry, and E. Joubert, "Thermal analysis of AlGaN/GaN high-electron mobility transistors using I-V pulsed characterizations and infra-red microscopy," *IEEE Trans. Device Mater. Rel.*, vol. 19, no. 4, pp. 704–710, Dec. 2019.

[19] S. Karboyan, J. Tartarin, and B. Lambert, "Analysis of barrier inhomogeneities in AlGaN/GaN HEMTs' Schottky diodes by I-V-T measurements," in *Proc. Eur. Microw. Integr. Circuit Conf.*, Jan. 2013, pp. 240–243.

[20] A. Stocco, "Reliability and failure mechanisms of GaN HEMT devices suitable for high-frequency and high-power applications," Ph.D. dissertation, Univ. Padua, Padua, Italy, 2012.

[21] J. Tartarin *et al.*, "Gate defects analysis in AlGaN/GaN devices by mean of accurate extraction of the Schottky barrier height, electrical modelling, T-CAD simulations and TEM imaging," *Microelectron. Rel.*, vol. 76–77, pp. 344–349, 2017.

[22] M. Dammann *et al.*, "Reliability status of GaN transistors and MMICs in Europe," in *Proc. IEEE Int. Rel. Phys. Symp.*, 2010, pp. 129–133.

[23] J. Joh, J. A. Del Alamo, U. Chowdhury, and J. L. Jimenez, "Correlation between RF and DC reliablity in GaN high electron mobility transistors," in *Proc. Rel. Compound Semicond. Workshop*, 2008, pp. 185–194.

[24] M. Dammann *et al.*, "Reliability and degradation mechanism of AlGaN/GaN HEMTs for next generation mobile communication systems," *Microelectron. Rel.*, vol. 49, no. 5, pp. 474–477, 2009.

[25] A. Sozza, C. Dua, E. Morvan, B. Grimber, and S. Delage, "A 3000 hours DC life test on AlGaN/GaN HEMT for RF and microwave applications," *Microelectron. Rel.*, vol. 45, no. 9, pp. 1617–1621, 2005.

[26] N. Moultif, A. Divay, E. Joubert, and O. Latry, "Localizing and analyzing defects in AlGaN/GaN HEMT using photon emission spectral signatures," *Eng. Failure Anal.*, vol. 81, pp. 69–78, 2017.

[27] G. Meneghesso *et al.*, "Trapping phenomena in AlGaN/GaN HEMTs: A study based on pulsed and transient measurements," *Semicond. Sci. Technol.*, vol. 28, no. 7, Jun. 2013, Art. no. 074021.

[28] O. Mitrofanov and M. Manfra, "Mechanisms of gate lag in GaN/AlGaN/GaN high electron mobility transistors," *Superlattices Microstruct.*, vol. 34, no. 1, pp. 33–53, 2003.

[29] J. M. Tirado, J. L. Sanchez-Rojas, and J. I. Izpura, "Trapping effects in the transient response of AlGaN/GaN HEMT devices," *IEEE Trans. Electron Devices*, vol. 54, no. 3, pp. 410–417, Mar. 2007.

[30] N. Braga, R. Mickevicius, R. Gaska, M. S. Shur, M. A. Khan, and G. Simin, "Simulation of gate lag and current collapse in gallium nitride field-effect transistors," *Appl. Phys. Lett.*, vol. 85, no. 20, pp. 4780–4782, 2004.

[31] X. Zhou *et al.*, "Impact of bulk traps in GaN buffer on the gate-lag transient characteristics of AlGaN/GaN HEMTs," *Solid-State Electron.*, vol. 100, pp. 15–19, Oct. 2014.
[32] J. G. Tartarin, "Diagnostic tools for accurate reliability investigations of GaN devices," in *Proc. 21st Int. Conf. Noise Fluctuations*, 2011, pp. 452–457.
[33] A. Arehart, A. Sasikumar, G. Via, B. Poling, E. Heller, and S. Ringel, "Evidence for causality between GaN RF HEMT degradation and the Ec-0.57eV trap in GaN," *Microelectron. Rel.*, vol. 56, pp. 45–48, 2016.
[34] F. Magnier, B. Lambert, C. Chang, A. Curutchet, N. Labat, and N. Malbert, "Investigation of trap induced power drift on $0.15\mu m$ GaN technology after aging tests," *Microelectron. Rel.*, vol. 100–101, 2019, Art. no. 113358.
[35] A. Malik *et al.*, "Role of AlGaN/GaN interface traps on negative threshold voltage shift in AlGaN/GaN HEMT," *Solid-State Electron.*, vol. 142, pp. 8–13, 2018.
[36] F. Danesin *et al.*, "Thermal storage effects on AlGaN/GaN HEMT," *Microelectron. Rel.*, vol. 48, no. 8, pp. 1361–1365, 2008.
[37] L. Richard *et al.*, "Reliability investigation of gallium nitride HEMT," *Microelectron. Rel.*, vol. 44, no. 9, pp. 1369–1373, 2004.
[38] S. N. Mohammad, "Contact mechanisms and design principles for Schottky contacts to group-III nitrides," *J. Appl. Phys.*, vol. 97, no. 6, 2005, Art. no. 063703.
[39] A. Soltani *et al.*, "Development and analysis of low resistance ohmic contact to n-AlGaN/GaN HEMT," *Diamond Related Mater.*, vol. 16, no. 2, pp. 262–266, 2007.
[40] M. Zhao, X. Wang, X. Liu, J. Huang, Y. Zheng, and K. Wei, "Thermal storage of AlGaN/GaN high-electron-mobility transistors," *IEEE Trans. Device Mater. Rel.*, vol. 10, no. 3, pp. 360–365, Sep. 2010.
[41] N. Killat, M. Ťapajna, M. Faqir, T. Palacios, and M. Kuball, "Evidence for impact ionisation in AlGaN/GaN HEMTs with InGaN back-barrier," *Electron. Lett.*, vol. 47, no. 6, pp. 405–406, Mar. 2011.
[42] E. Zanoni *et al.*, "Reliability of gallium nitride microwave transistors," in *Proc. 21st Int. Conf. Microw., Radar Wireless Commun.*, May 2016, pp. 1–6.
[43] C. Hodges *et al.*, "Optical investigation of degradation mechanisms in AlGaN/GaN high electron mobility transistors: Generation of non-radiative recombination centers," *Appl. Phys. Lett.*, vol. 100, no. 11, 2012, Art. no. 112106.
[44] P. Marko *et al.*, "IV, noise and electroluminescence analysis of stress-induced percolation paths in AlGaN/GaN high electron mobility transistors," *Microelectron. Rel.*, vol. 52, no. 9, pp. 2194–2199, 2012.
[45] M. Ťapajna, N. Killat, U. Chowdhury, J. L. Jimenez, and M. Kuball, "The role of surface barrier oxidation on AlGaN/GaN HEMTs reliablity," *Microelectron. Rel.*, vol. 52, no. 1, pp. 2–32, 2012.
[46] P. Ivo *et al.*, "Comparative study of AlGaN/GaN HEMTs robustness versus buffer design variations by applying electroluminescence and electrical measurements," *Microelectron. Rel.*, vol. 51, no. 2, pp. 217–223, 2011.
[47] A. Glowacki, C. Boit, R. Lossy, and J. Wuerfl, "Photon emission spectral signatures of AlGaN/GaN HEMT for functional and Reliablity analysis," in *Proc. 34th Int. Symp. Testing Failure Anal.*, Portland, OR, USA, Nov. 2008, pp. 220–226.
[48] L. Stuchlìkovà *et al.*, "Electrical characterization of the InAlN/GaN heterostructures by capacitance methods," in *Proc. 9th Int. Conf. Adv. Semicond. Devices Mircosystems*, Nov. 2012, pp. 51–54.
[49] A. R. Arehart, A. A. Allerman, and S. A. Ringel, "Electrical characterization of n-type $Al_{0.30}Ga_{0.70}N$ Schottky diodes," *J. Appl. Phys.*, vol. 109, no. 11, 2011, Art. no. 114506.
[50] A. C. Malonis, "Quantitative defect spectroscopy on operating AlGaN/GaN high electron mobility transistors," Ph.D. dissertation, Ohio State Univ., Columbus, OH, USA, 2009.
[51] N. Shigekawa, K. Shiojima, and T. Suemitsu, "Electroluminescence characterization of AlGaN/GaN high-electron-mobility transistors," *Appl. Phys. Lett.*, vol. 79, no. 8, pp. 1196–1198, 2001.
[52] A. Hierro, S. A. Ringel, M. Hansen, J. S. Speck, U. K. Mishra, and S. P. DenBaars, "Hydrogen passivation of deep levels in n–GaN," *Appl. Phys. Lett.*, vol. 77, no. 10, pp. 1499–1501, 2000.
[53] A. R. Arehart *et al.*, "Comparison of deep level incorporation in ammonia and RF-plasma assisted molecular beam epitaxy n-GaN films," *Physica Status Solidi C*, vol. 5, no. 6, pp. 1750–1752, 2008.
[54] A. R. Arehart, T. Homan, M. H. Wong, C. Poblenz, J. S. Speck, and S. A. Ringel, "Impact of N- and Ga-face polarity on the incorporation of deep levels in n-type GaN grown by molecular beam epitaxy," *Appl. Phys. Lett.*, vol. 96, no. 24, 2010, Art. no. 242112.